A novel Design Approach of a Micro Thermoelectric Generator for High Power Density for Ambient Heat Energy Scavenging Applications.

Donart Nayebare[1,*], Ahmed M.R Fath El-Bab[2], Tamer F. Megahed[1,4], Asano Tanemasa[3] and Sobhy M. Abdelkader[1,4]

[1] Electrical Power Engineering Department, Egypt-Japan University of Science and Technology (E-JUST), Egypt
[2] Mechatronics and Robotics Engineering Department, Egypt-Japan University of Science and Technology (E-JUST), Egypt
[3] Graduate School of Information Science and Electrical Engineering, Kyushu University, Fukuoka, Japan
[4] Electrical Engineering Department, Mansoura University, El-Mansoura 35516, Egypt
* Corresponding author: donart.nayebare@ejust.edu.eg

Abstract. Thermoelectric generators (TEGs) have become an excellent candidate for autonomously powering wearable and implantable microelectronics, and wireless sensor networks in the Internet of Things (IoT) systems. This paper presents a double-layer double-circuit planar TEG with high power output. The impact of the different geometric terms on the device performance is investigated by the use of an electrical model. By studying the impact of the width of the TE films, the number of pairs is optimized to give the optimal power output. The impact of increasing the number of pairs on the output variables of the TEG is also studied. The maximum power of 0.522µW was obtained from 32 pairs at a metal width of 3.82mm with a temperature difference of 17K. Further improvement in the output power up to mW can be obtained by optimizing the temperature difference and operating in a temperature range of about 450K, such as in industrial heat recovery applications.

Key words. Energy Scavenging, Wearable, Implantable, Internet of Things, Double layer, Double Circuit, and Planar.

1. Introduction

Recently, there is an increasing trend for small-scale wearable and implantable electronic devices [1], [2], especially for health and wellness monitoring. With the evolution of the Internet of Things (IoT), in which sensors and wireless devices can interact to exchange information[3]–[5], the globe will be further connected and more intelligent.

The combination of the IoT and wearable electronics will enhance communication between mankind, Wireless Sensor Networks (WSN), and the surroundings, in a more seamless manner [6].

Nevertheless, this will be possible with a more reliable and continuous power supply unlike the use of batteries, which require periodic recharging and replacement. There are several techniques for harvesting micro-energy from the surroundings, including solar-based devices [7], piezoelectric [8], triboelectric [9], and notably thermoelectric (TE) [10]–[12]. TE generators (TEGs) have more promising applications in wearable (or small-scale) electronics [12], [13] since heat is ubiquitous and does not rely on any mechanical input or light, unlike other sources

such as piezoelectric. They produce power directly from any heat source. Moreover, TEGs are renewable, with no moving parts hence high reliability [10], and noiseless. Although TEGs produce small quantities of power in micro-Watts, it has been proven to be sufficient to power most portable electronics such as wireless sensors [2], [14]–[16], and implantable electronics such as Cardiac PaceMaker [16].

However, TE is limited by low efficiency which is determined by the thermoelectric dimensionless figure of merit (ZT), given by: $ZT = \frac{S^2}{\rho k} T$

Where S is the Seebeck coefficient, k is thermal conductivity, ρ is the electrical resistivity, and T is the absolute temperature. Thus, many researchers have focused on the development and characterization of new materials with a high ZT and less on device fabrication [17]

There is still a challenge in fabricating a microscale TEG with a high-power density. In this work, geometry optimization at a device level has been undertaken. Though much better results can be obtained if simultaneous optimization of the material properties, device, and system is done. A planar configuration is preferred over the vertical type. It is simple to fabricate because there is no bonding process required [11], and is suitable for low-cost mass production since less material is needed.

Shen et al. [11] proposed a planar TEG with a circular pattern. In their design, Cu electrodes with dimensions bigger than the TE legs themselves were used as a means of interconnecting the TE legs which would increase the material requirement and the parasitic contact electrical resistance. Chen et al. [1] proposed a novel multi-layer design in which each TE metal is set to layer by layer but didn't carry out any numerical study to verify their findings. Pelegrini et al. [18] proposed a double circuit design and obtained promising results but did not utilize the multilayer concept used in the present paper. Leon et al. [19] and Peng et al. [20] both suggested planar circular patterns and used CMOS and Micro-ElectroMechanical Systems (MEMS) processes to design and fabricate micro-TEGs with promising results.

Many researchers in this field have used a vertical configuration [2], [12], [13], [21], but the cross-plane design has limitations of short leg length due to aesthetics, hence small thermal gradient, and the need for the bonding process to anchor the connectors to the TE legs. Wang et al. [22] conducted a comprehensive analytical model to investigate the impact of geometric parameters on the output metrics of the TEG. However, in their study, they considered a single TE pair of the vertical configuration. To the best of the authors' knowledge, no such inclusive geometric study, in terms of the output power, has been conducted on the planar type of TEG before.

In this work, a double layer-double circuit planar TEG with rectangular TE legs is introduced, as shown in Fig. 1, where each metal circuit utilizes a layer, separated by a thin insulating film, and interconnected to form pairs through small contact holes. The proposed design allows the device to have a huge number of TE pairs in the smallest possible substrate area. A comprehensive geometric analysis has been conducted to investigate the effect of different geometric terms and dimensions on the performance metrics of the generator. An electrical model that expresses the power output in terms of the device geometry was used in the study.

2. Working Principle of a TEG

According to the Seebeck effect, a TEG generates electricity directly from heat. When junctions of two dissimilar metals *a* and *b* are subjected to a thermal gradient, such that one junction is hot and the other cold, an emf is induced [23], as shown in Fig. 2.
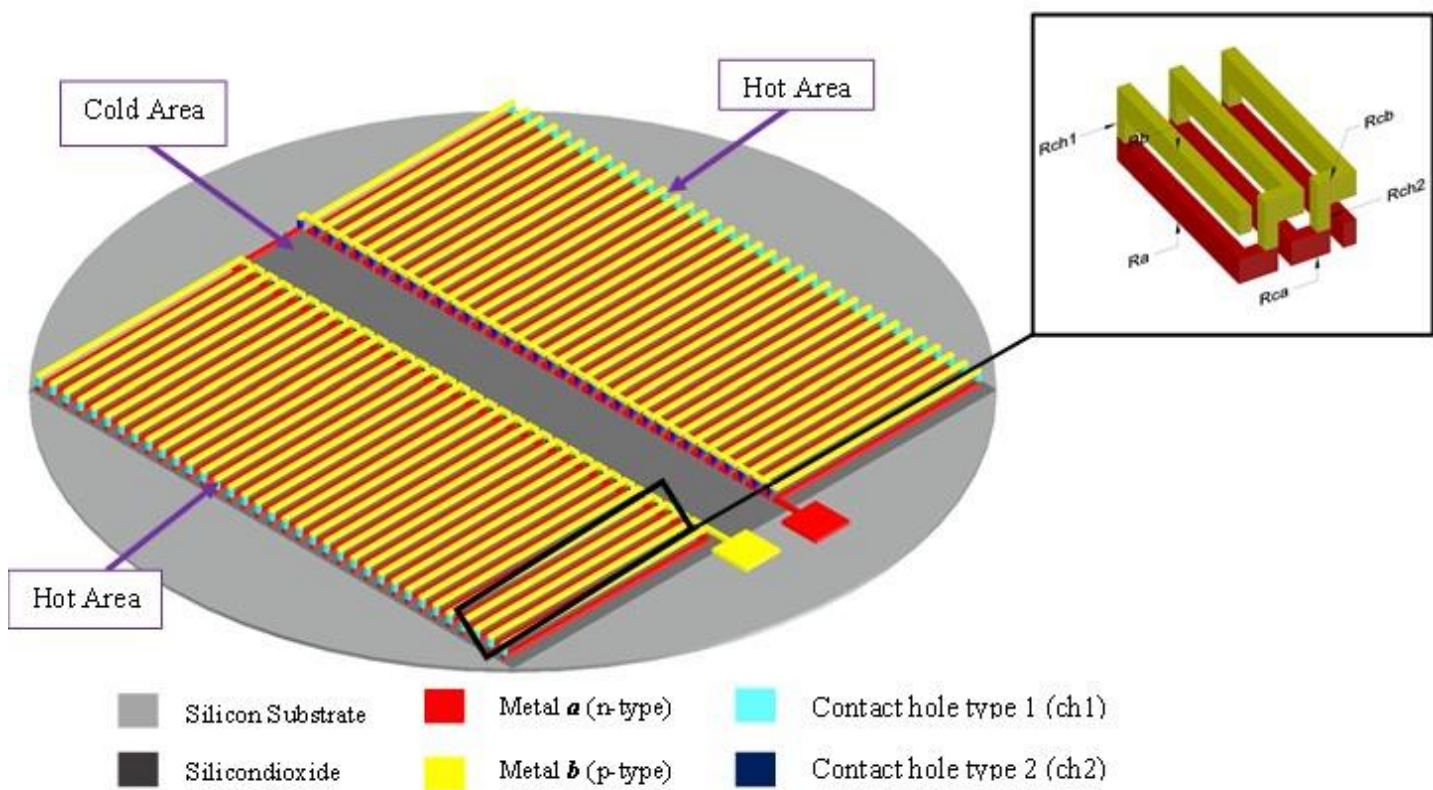
Fig. 1. Schematic Diagram (Isometric View) of the Double-layer Double circuit Planar TEG
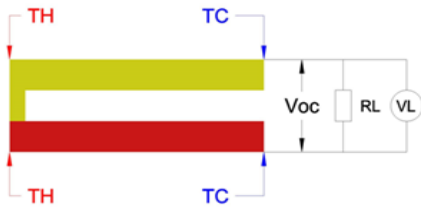
Fig. 2. Schematic Illustration (x-z plane) of a Double-layer Planar Thermoelectric Couple (TEC)

The thermoelectric open-circuit voltage (V_{oc}) induced is a function of the Seebeck coefficients of the thermoelements and the temperature difference, given by the following expression:

$$V_{oc} = \int_{T_C}^{T_H} (S_a(T) - S_b(T))\, dT \tag{1}$$

where S_a and S_b are Seebeck coefficients of thermoelements a and b, T_H and T_C are temperatures of the hot side and cold side junctions respectively.

Seebeck coefficient is a function of the temperature. It is non-linear and depends on the thermoelement's absolute temperature, material properties, and molecular structure.

If the Seebeck coefficients are effectively constant for the measured temperature range, then eqn. (1) becomes:

$$V_{oc} = (S_a - S_b)(T_H - T_C) = S\Delta T \tag{2}$$

where S is the relative Seebeck coefficient of the thermoelectric couple and ΔT is the temperature difference
If an external load of resistance R_L is connected across the TEC, the current flowing, I_L is given by:

$$I_L = \frac{V_{oc}}{R_i + R_L} \tag{3}$$

where V_L is the load voltage and R_i is the steady-state internal electrical resistance of the TEC, given by:

$$R_i = \frac{\rho L}{A} \tag{4}$$

The power flowing through the load is then expressed as:

$$P_L = I_L{}^2 R_L \tag{5}$$

$$P_L = \left(\frac{V_{oc}}{R_i + R_L}\right)^2 R_L \tag{6}$$

For maximum power point tracking (MPPT), the load resistance R_L must match the internal resistance of the generator (i.e., $R_L = R_i$) [19], [24], [25].

$$P_{MPPT} = \frac{V_{oc}{}^2}{4R_i} = \frac{(S\Delta T)^2}{4R_i} \tag{7}$$

Eqn. (7) is the maximum thermoelectric power that can be generated from one pair.
To optimize the power, it is desirable to maximize voltage while minimizing the internal resistance of the generator.
The thermoelectric output voltage depends on the Seebeck coefficient and temperature difference. Seebeck coefficient is a material property of the thermoelements, and its enhancement is outside the scope of this work.
In this work, TE materials commercially available in the market are utilized.
The internal resistance R_i depends on the geometrical terms such as the length and width of the TE legs.
This work, therefore, focuses on optimizing the geometry and the design to fabricate an optimal-power density μTEG.

3. Materials and Methods

A. The Electrical Model

The voltage, resistance, and power of the device can be expressed in terms of geometry.
For *N* pairs connected electrically in series and thermally in parallel such that one side is heated, and the other is cooled:
The generator open circuit voltage V_{TEG} becomes:

$$V_{TEG} = NV_{oc} = NS\Delta T \tag{8}$$

The internal resistance R_i of one repeatable TEC consists of R_a from metal *a*, R_b from metal *b*, R_{ca} of contact contributed by metal *a*, R_{cb} of contact contributed by metal *b*, R_{ch1}, and R_{ch2} of the two contact hole types.

$$R_i = R_a + R_b + R_{ca} + R_{cb} + R_{ch1} + R_{ch2} \tag{9}$$

Neglecting the resistance of the electrical pads, terminal connection to the pads, and the connection between the two parallel sets of thermopiles.
The total internal resistance, R_{TEG}, of the generator will be:

$$R_{TEG} = NR_i = N(R_a + R_b + R_{ca} + R_{cb} + R_{ch1} + R_{ch2}) \tag{10}$$

The power output of one pair in eqn. (7), in terms of the geometry, can be expressed as:

$$P_{MPPT} = \frac{V_{oc}^2}{4(R_a + R_b + R_{ca} + R_{cb} + R_{ch1} + R_{ch2})} \tag{11}$$

Assuming ideal operating conditions where there are no thermal variations between the different TECs, such that all TECs experience an equal ΔT [24].
The generator power output PTEG becomes:

$$P_{TEG} = NP_{MPPT} \tag{12}$$

$$P_{TEG} = N\left(\frac{(S\Delta T)^2}{4(R_a + R_b + R_{ca} + R_{cb} + R_{ch1} + R_{ch2})}\right) \quad (13)$$

The resistances R_a, R_b, R_{ca}, R_{cb}, R_{ch1}, and R_{ch2} can be expressed in terms of the geometry and resistivity ρ as given in eqn. (4)

The total contact length consists of L_{ca} of metal a and L_{cb} of metal b, overlapping by a pre-defined contact hole length, L_{ch2} for effective contact bonding.

The contact holes will be of material b, deposited from the upper layer.

Accordingly,

$$R_a = \frac{\rho_a L_a}{A_a}, R_b = \frac{\rho_b L_b}{A_b}, \ R_{ca} = \frac{\rho_a L_{ca}}{A_{ca}},$$
$$R_{cb} = \frac{\rho_b L_{cb}}{A_{cb}}, R_{ch1} = \frac{\rho_b t_{ch1}}{A_{ch1}}, \text{and} \quad (14)$$
$$R_{ch2} = \frac{\rho_b t_{ch2}}{A_{ch2}}$$

L_a, L_b, A_a, and A_b are the lengths and cross-section areas of the thin-films of metals a and b, while L_{ca}, L_{cb}, t_{ch1}, t_{ch2}, A_{ca}, A_{cb}, A_{ch1}, and A_{ch2}, the lengths, thicknesses, and cross-section areas of interconnecting contacts contributed by metal a, metal b and contact hole type-1 and 2 respectively. Contact hole type 1 connects metal a to metal b to create pairs while type 2 connects pairs to form the series connections.

As shown in Fig. 1, in-plane legs with a lateral heat flow are employed in this work. However, it is important to note that the contact hole is vertical.

Hence, the cross-section area (or the heat transfer area) of the metal films and contacts is width by thickness, while that of the contact holes is width by length, expressed as follows:

$$A_a = w_a t_a, A_b = w_b t_b, A_{ca} = w_{ca} t_{ca},$$
$$A_{cb} = w_{cb} t_{cb}, A_{ch1} = w_{ch1} L_{ch1}, and \quad (15)$$
$$A_{ch2} = w_{ch2} L_{ch2}$$

where w_a, w_b, w_{ca}, w_{cb}, w_{ch1}, w_{ch2}, t_a, t_b, t_{ca}, t_{cb}, L_{ch1}, and L_{ch2} are the widths, thicknesses, and lengths of the metal films, contacts, and contact holes respectively

Substituting eqns. (14) and (15) into eqn. (13) yields:

$$P_{TEG} = N\left(\frac{(S\Delta T)^2}{4\left(\begin{array}{c}\frac{\rho_a L_a}{w_a t_a} + \frac{\rho_b L_b}{w_b t_b} + \frac{\rho_a L_{ca}}{w_{ca} t_{ca}} + \\ \frac{\rho_b L_{cb}}{w_{cb} t_{cb}} + \frac{\rho_b t_{ch1}}{w_{ch1} L_{ch1}} + \frac{\rho_b t_{ch2}}{w_{ch2} L_{ch2}}\end{array}\right)}\right) \quad (16)$$

The legs of metal a and b are designed to have similar dimensions as seen in Table 2. The contacts of metal a and b are also designed to have identical dimensions. The contacts and the metal legs will have the same thickness. The lengths and thicknesses of the contact holes-1 and 2 will be similar by design. However, the width of contact hole-1 must be equal to the width of the metal legs, and the width of contact hole-2 must be equal to the width of the contacts.

Therefore, $L_a = L_b = L$, $w_a = w_b = w_{ch1} = w$, $t_a = t_b = t_{ca} = t_{cb} = t$, $L_{ca} = L_{cb} = L_c$, $w_{ca} = w_{cb} = w_{ch2} = w_c$, $L_{ch1} = L_{ch2} = L_{ch}$, and $t_{ch1} = t_{ch2} = t_{ch}$.

Then equation 16 simplifies to:

$$P_{TEG} = N\left(\frac{(S\Delta T)^2}{4\left(\begin{array}{c}\frac{\rho_a L}{wt} + \frac{\rho_b L}{wt} + \frac{\rho_a L_c}{w_c t} + \frac{\rho_b L_c}{w_c t} + \\ \frac{\rho_b t_{ch}}{w L_{ch}} + \frac{\rho_b t_{ch}}{w_c L_{ch}}\end{array}\right)}\right) \quad (17)$$

Eqn. (17) represents the power of the micro thermoelectric generator as a function of the inherent material properties of the thermoelements and geometric terms.

B. *Material Properties*

Materials with high thermoelectric properties at room temperature were considered. Tellurium alloys, n-type Bismuth Telluride and p-type Antimony Telluride are the best reported and well-established room temperature TE materials [10], [21].

Table 1: Materials and their Properties

Material Name	Thermal conductivity (W/ (m K))	Electrical Resistivity (Ω m)	Seebeck Coefficient (µV/K)
Bismuth	8	1.3×10^{-6}	-77
Antimony	24	4×10^{-7}	42
Tellurium	3	0.0001	495
n-type Bismuth Telluride	1.3	10.6×10^{-6}	-235
p-type Antimony Telluride	1.8	12.6×10^{-6}	180

C. *Numerical Analysis*

Various analyses of the output metrics (i.e., power output, load current, voltage, and resistance) against the different geometry inputs (such as the area, width, length, thickness, contact hole dimensions, and the number of pairs) can be studied, according to eqns. (8), (10), and (17).

In this paper, we will focus on the impact factor of increasing N (which is a function of w, according to eqn. (19)), on the output voltage, current, and power versus the resistance.

Even though, a higher N will increase the voltage and hence the power, its effect on the internal resistance of the device is detrimental [25].

To study this, we varied the width w from 200µm to 70700µm and kept other terms constant as shown in Table 2. According to our model, only the width of the metal films and contact length affect the number of pairs that can be connected in series.

By changing the width w of the TE legs in eqn. (17) and keeping all the other terms constant and known, yields:

$$P_{TEG} = \frac{N}{4}\left(\frac{d}{\frac{e}{w}+f}\right) \qquad (18)$$

d, e, and *f* are constants
The denominator in parenthesis is the resistance of one pair.

Subject to:

$$N = \frac{0.1414}{w+g} \qquad (19)$$

w is the width of the metal and g is the gap between two pairs given by $g = 2L_c - L_{ch2}$.
w and *N* are constrained by the total width of the effective substrate area

D. Results and discussion

1) Effect of varying w on N and R
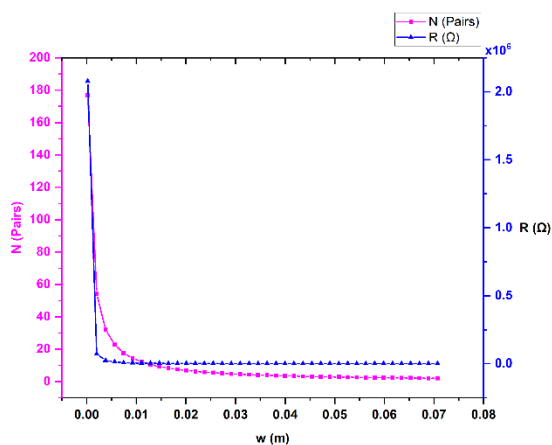
Fig. 3. Effect of varying *w* on *N* and *R*

Both the number of pairs *N* and resistance *R* reduce as *w* increases according to eqns. (19) and (18) respectively and become almost constant as *w* approaches maximum. This phenomenon is shown in Fig. 3.

2) The effect of varying w on the Power
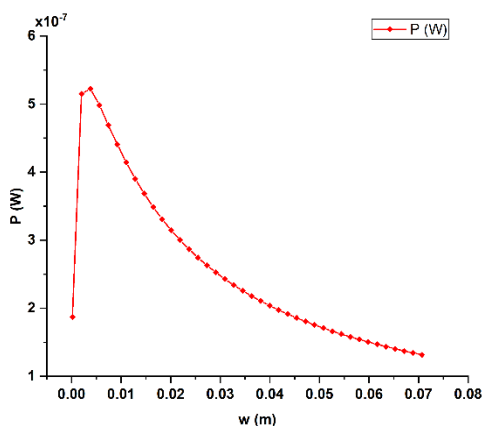
Fig. 4. Variation of Power against *w*

The power increases as *w* increases according to eqn. (**18**). This trend is shown in Fig. 4. Increasing *w* increases power

and reduces *N* yet power and *N* are directly proportional. This means that there is an optimal value of *w* hence an optimum number of pairs. This behavior is explained in part 3 of the results in Fig. 5.

3) The effect of varying N on the Power, Voltage, and Resistance
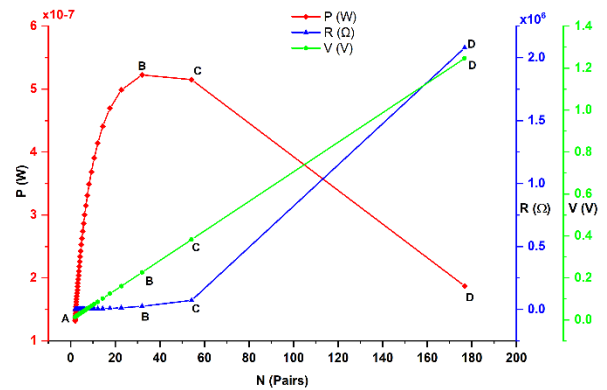
Fig. 5. Variation of the Power, Voltage, and Resistance against *N*

According to Fig**.** 5, the effect of increasing the number of pairs on each of the generator output metrics was analyzed as follows:

Part A-B: The power increases as *N* increases. The number of pairs is increased from 2 at point A to 32 at point B, while the output power increases by 296.9% from 1.32×10^{-07} W to 5.22×10^{-07} W. The resistance increases by about 6470% from 371.8Ω to $2.44 10^{04}$Ω. The voltage has a linear relationship with N according to eqn. (**8**). It increased by 1515% from 0.014V to 0.226V.
Part B-C. The power starts to decrease as *N* continues to increase, while the resistance and voltage continue increasing. The percentage decrease in power in this region is about 1.4% while the voltage and resistance increased by 69.3% and 190.9% respectively
In region C-D, the power further decreased at the rate of 63.7%. The voltage and resistance increased by 226% and 2824.4% respectively.

In all the regions, the resistance has the biggest rate of increase as N is increased. Therefore, while increasing the number of pairs in series has a positive effect and increases the power and voltage, its impact on the internal resistance of the generator is extremely adverse.
Hence, an optimal value of *N* must be obtained and used. From the graph, point B should be the optimum point. However, in the region between B-C, whereas the power decreases, its decrease is minor (only 1.4%) from 5.22×10^{-07} W to 5.15×10^{-07} W, compared to the increase in voltage by 69.3%.
Therefore, a tradeoff between the power and voltage was taken, and C was chosen as the optimal point corresponding to *N* equal to 54 pairs and a width, *w* of approximately 2000μm.

Table 2-Parameters used in Numerical Analysis

Description	Symbol	Values (μm)
Metal length	**L**	30000
Metal width	**w**	200
Metal thickness	**t**	0.3
Contact length	**L$_c$**	400
Contact width	**w$_c$**	200
Contact thickness	**t$_c$**	0.3
Contact hole-Type 1		
length	**L$_{ch1}$**	200
width	**w$_{ch1}$**	200
thickness	**t$_{ch1}$**	0.2
Contact hole-Type 2		
length	**L$_{ch2}$**	200
width	**w$_{ch2}$**	200
thickness	**t$_{ch2}$**	0.2
Effective gap width between 2 pairs	**g**	600
Electrical Pad length		5000
Electrical Pad width		5000
Electrical Pad thickness		0.3
Length of the connection to the pad		3000
The gap width between set 1 & set 2 thermopiles		9700

4. Conclusion

In this work, a new design with a high power output has been introduced. The impact of geometric terms on the performance of the thermoelectric device was successfully examined using the electrical model. The thermoelement width was varied and an optimum value for maximum power was determined. The maximum power of 0.522μW was obtained for just 32 pairs corresponding to a metal width of 3.82mm and a temperature difference of 17K. The analysis further indicates that if the temperature difference is optimized up to 450K, the power in the order of mW can be achieved.

Acknowledgement

References

[1] T. Chen, Z. Zheng, G. Liang, and P. Fan, "A new design of a thin-film thermoelectric device based on multilayer-structure module," *Nanomaterials*, vol. 10, no. 5. MDPI AG, May 01, 2020. doi: 10.3390/nano10050990.

[2] D. N. Kossyvakis, S. G. Vassiliadis, C. G. Vossou, E. E. Mangiorou, S. M. Potirakis, and E. v. Hristoforou, "Computational Analysis of a Thermoelectric Generator for Waste-Heat Harvesting in Wearable Systems," *Journal of Electronic Materials*, vol. 45, no. 6, pp. 2957–2966, Jun. 2016, doi: 10.1007/s11664-016-4452-2.

[3] D. Giusto, A. Iera, G. Morabito, and L. Atzori, Eds., *The Internet of Things*. New York, NY: Springer New York, 2010. doi: 10.1007/978-1-4419-1674-7.

[4] S. Hiremath, G. Yang, and K. Mankodiya, "Wearable Internet of Things: Concept, Architectural Components and Promises for Person-Centered Healthcare," Dec. 2014. doi: 10.4108/icst.mobihealth.2014.257440.

[5] M. Swan, "Sensor mania! the internet of things, wearable computing, objective metrics, and the quantified self 2.0," *Journal of Sensor and Actuator Networks*, vol. 1, no. 3. MDPI AG, pp. 217–253, Dec. 01, 2012. doi: 10.3390/jsan1030217.

[6] A. Nozariasbmarz *et al.*, "Review of wearable thermoelectric energy harvesting: From body temperature to electronic systems," *Applied Energy*, vol. 258. Elsevier Ltd, Jan. 15, 2020. doi: 10.1016/j.apenergy.2019.114069.

[7] B. J. Kim *et al.*, "Highly efficient and bending durable perovskite solar cells: Toward a wearable power source," *Energy and Environmental Science*, vol. 8, no. 3, pp. 916–921, Mar. 2015, doi: 10.1039/c4ee02441a.

[8] IEEE Staff, *2017 19th International Conference on Solid State Sensors, Actuators and Microsystems (TRANSDUCERS)*. IEEE, 2017.

[9] S. Wang *et al.*, "An integrated flexible self-powered wearable respiration sensor," *Nano Energy*, vol. 63, Sep. 2019, doi: 10.1016/j.nanoen.2019.06.025.

[10] J. P. Carmo, L. M. Goncalves, R. F. Wolffenbuttel, and J. H. Correia, "A planar thermoelectric power generator for integration in wearable microsystems," *Sensors and Actuators, A: Physical*, vol. 161, no. 1–2, pp. 199–204, Jun. 2010, doi: 10.1016/j.sna.2010.05.010.

[11] H. Shen, H. Lee, and S. Han, "Optimization and fabrication of a planar thermoelectric generator for a high-performance solar thermoelectric generator," *Current Applied Physics*, vol. 22, pp. 6–13, Feb. 2021, doi: 10.1016/j.cap.2020.11.005.

[12] F. Suarez, A. Nozariasbmarz, D. Vashaee, and M. C. Öztürk, "Designing thermoelectric generators for self-powered wearable electronics," *Energy and Environmental Science*, vol. 9, no. 6, pp. 2099–2113, Jun. 2016, doi: 10.1039/c6ee00456c.

[13] A. Nozariasbmarz *et al.*, "High Power Density Body Heat Energy Harvesting," *ACS Applied Materials and Interfaces*, vol. 11, no. 43, pp. 40107–40113, Oct. 2019, doi: 10.1021/acsami.9b14823.

[14] M. T. Dunham, M. T. Barako, S. LeBlanc, M. Asheghi, B. Chen, and K. E. Goodson, "Power density optimization for micro thermoelectric generators," *Energy*, vol. 93, pp. 2006–2017, 2015, doi: 10.1016/j.energy.2015.10.032.

[15] M. Falk *et al.*, "Self-powered wireless carbohydrate/oxygen sensitive biodevice based on radio signal transmission," *PLoS ONE*, vol. 9, no. 10, Oct. 2014, doi: 10.1371/journal.pone.0109104.

[16] Universiti Teknologi PETRONAS, TechSource Systems, IEEE Malaysia Section, Institute of Electrical and Electronics Engineers., and S. & T. C. (2016 : K. L. World Engineering, *ICIAS 2016 : International Conference on Intelligent and Advanced Systems : Technological Convergence for a Sustainable Future : 15-17 August 2016, Kuala Lumpur Convention Centre*.

[17] N. W. Park *et al.*, "Thermoelectric characterization and fabrication of nanostructured p-type Bi0.5Sb1.5Te3 and n-type Bi2Te3 thin film thermoelectric energy generator with an in-plane planar structure," *AIP Advances*, vol. 6, no. 6, Jun. 2016, doi: 10.1063/1.4955000.

[18] S. Pelegrini *et al.*, "Development and characterization of a microthermoelectric generator with plated copper/constantan thermocouples," in *Microsystem*

Technologies, 2014, vol. 20, no. 4–5, pp. 585–592. doi: 10.1007/s00542-013-1993-7.

[19] M. T. de Leon, H. Chong, and M. Kraft, "Solar thermoelectric generators fabricated on a silicon-on-insulator substrate," *Journal of Micromechanics and Microengineering*, vol. 24, no. 8, Aug. 2014, doi: 10.1088/0960-1317/24/8/085011.

[20] S. W. Peng, P. J. Shih, and C. L. Dai, "Manufacturing and characterization of a thermoelectric energy harvester using the CMOS-MEMS technology," *Micromachines*, vol. 6, no. 10, pp. 1560–1568, 2015, doi: 10.3390/mi6101439.

[21] A. Nozariasbmarz *et al.*, "Thermoelectric generators for wearable body heat harvesting: Material and device concurrent optimization," *Nano Energy*, vol. 67, Jan. 2020, doi: 10.1016/j.nanoen.2019.104265.

[22] L. Wang *et al.*, "Modeling the effects of module size and material property on thermoelectric generator power," *ACS Omega*, vol. 5, no. 46, pp. 29844–29853, Nov. 2020, doi: 10.1021/acsomega.0c03914.

[23] G. de Pasquale, "Energy harvesters for powering wireless systems," in *Handbook of Mems for Wireless and Mobile Applications*, Elsevier Inc., 2013, pp. 345–400. doi: 10.1533/9780857098610.2.345.

[24] A. Montecucco, J. Siviter, and A. R. Knox, "The effect of temperature mismatch on thermoelectric generators electrically connected in series and parallel," *Applied Energy*, vol. 123, pp. 47–54, Jun. 2014, doi: 10.1016/j.apenergy.2014.02.030.

[25] N. Jaziri, A. Boughamoura, J. Müller, B. Mezghani, F. Tounsi, and M. Ismail, "A comprehensive review of Thermoelectric Generators: Technologies and common applications," *Energy Reports*, vol. 6. Elsevier Ltd, pp. 264–287, Dec. 01, 2020. doi: 10.1016/j.egyr.2019.12.011.